Spectral shifts and asymmetries in mid-infrared assisted high-order harmonic generation

Balázs Major[1,2,*], **Emeric Balogh**[1,*], **Katalin Kovács**[3], **Songhee Han**[4], **Bernd Schütte**[4], **Paul Weber**[4], **Marc J. J. Vrakking**[4], **Valer Tosa**[3], **Arnaud Rouzée**[4], and **Katalin Varjú**[1,2,**]

[1] *Department of Optics and Quantum Electronics, University of Szeged, P.O. Box 406, Szeged 6701, Hungary*
[2] *ELI-ALPS, ELI-HU Non-Profit Ltd., Dugonics ter 13, Szeged 6720, Hungary*
[3] *National Institute for R&D of Isotopic and Molecular Technologies, Donath 67-103, 400293 Cluj-Napoca, Romania*
[4] *Max-Born-Institut, Max-Born-Strasse 2A, 12489 Berlin, Germany*
[*] *These authors contributed equally to this work.*
[**] *Corresponding author: katalin.varju@eli-alps.hu*

We study high-order harmonics generated by an intense multicycle 800 nm laser pulse in the presence of a weaker 1300 nm mid-infrared (MIR) pulse. Additionally to the previously observed effects of yield enhancement, cutoff extension and continuum generation, we report here a spectral shift of harmonic peaks controlled by the delay of the MIR pulse. We explain this effect considering the half-cycle to half-cycle behavior of the two-color field.   © 2018 Optical Society of America

OCIS codes: (190.4160) Multiharmonic generation; (320.7120) Ultrafast phenomena; (340.7480) X-rays, soft x-rays, extreme ultraviolet (EUV).

1. INTRODUCTION

High-order harmonic generation (HHG) in gases is a quickly developing research area [1–3], due to the fact that it enables the generation of the shortest controllably reproducible light pulses available for time-resolved spectroscopy [4, 5]. This tool allows to perform time-resolved studies on electronic processes in atoms, molecules, nanoparticles, liquids and solids on the attosecond timescale [6, 7] and to investigate in real time fundamental phenomena like photoemission, Auger decay or charge migration [8–11]. The applicability of these sources in time-resolved spectroscopic experiments depends on our ability to control the properties of the produced radiation [5]. Therefore, an understanding of the possible control knobs within the process is important not just because it broadens our knowledge about HHG, but also because it can provide additional opportunities for control in experiments.

Nonlinear optical processes can exhibit an intensity-dependent phase response. A well-known example is self-phase modulation (SPM) resulting from the third-order susceptibility, which causes an intense laser pulse propagating through a nonlinear medium to experience a frequency redshift at its leading edge and a blueshift at the trailing edge [12]. Since HHG is a highly nonlinear phenomenon, the phase of the generated radiation is also influenced by such intensity-dependent effects. For multicycle driving fields, the half-cycle periodicity of the harmonic generation process leads to the appearance of odd harmonic peaks in the spectrum, although a continuum

spectrum is generated in each identical half-cycle. For short generating pulses the effective intensity in consecutive half-cycles may be considerably different, and due to the linear relationship between the harmonic phase and the intensity, the harmonics experience a blueshift (redshift) on the rising (falling) part of the generating pulse [13]. This chirp of the individual harmonics has been observed and measured experimentally [14], and it has been connected to the varying spacing of the attosecond bursts in the pulse train [15].

When two intense laser beams propagate through a medium, nonlinear optical processes can result in the appearance of cross-terms, like wave-mixing or cross-phase modulation (XPM). In XPM one beam affects the phase of the other beam by modifying the optical properties of the medium, analogously to the SPM mechanism [12]. Similar effects can occur in two-color HHG. HHG by two different color fields has been widely studied since the 1990s [16], focusing on the generation of even [17] or circularly polarized harmonics [18, 19], as well as on the possibilities to increase the harmonic cutoff energy [20, 21] or harmonic yield [21–23]. The effects of an assisting pulse and its temporal delay with respect to the primary pulse have also been studied in relation to the temporal properties of the generated attosecond pulse train [24], in connection with interference of radiation from different trajectories [25], or in the context of phase matching [26].

In this paper we discuss the control of harmonic frequency shifts, which are a consequence of the combined application

of a near-infrared (NIR) and a mid-infrared (MIR) laser field for HHG. In previous experiments it has been shown that the additional (usually weaker) MIR field can extend the cutoff [20, 27], can reduce the number of generated attosecond pulses via two-color gating [27, 28], and can increase the harmonic yield [20, 21, 23, 27, 28]. Here we present experimental results and theoretical explanations of redshifted harmonics, increase / decrease of the harmonic yield at different delays between the pulses, and the generation of continuum radiation by multicycle pulses. Our investigation shows that fine tunability of the HHG spectrum is possible using a two-color laser scheme, therefore adding one control knob to the existing HHG toolbox.

2. EXPERIMENTAL AND MODELING

A. Experimental setup

Our experimental setup was based on a Ti:Sapphire amplifier, generating 35 fs pulses with up to 30 mJ energy at 50 Hz repetition rate. This NIR (800 nm) beam was split into two, and 20 mJ was used in a commercial optical parametric amplifier (HE-TOPAS from Light Conversion) to generate MIR (1300 nm) light with pulse energies up to 4 mJ (see Fig. 1). The delay between the MIR and the remaining NIR pulses was controlled with a motorized delay stage in step of 6.7 fs.
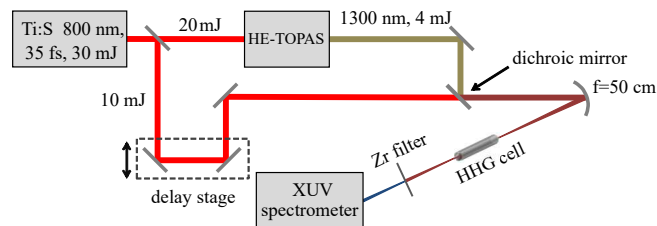

Fig. 1. Schematic illustration of the experimental setup.

The two beams were combined with a 45° dichroic mirror, and focused with the same $f = 50$ cm spherical mirror into a gas cell filled with neon at up to 700 mbar pressure. The NIR pulse duration was optimized for efficient MIR generation, and the dispersion in air and in the transmissive optical elements (beam splitter, dichroic mirror, vacuum window) caused a lengthening of the pulses to an estimated 50 fs on-target duration for both pulses. After the conversion process, a Zr filter blocked the NIR and MIR pulses, while harmonics from 70 to 200 eV were transmitted to the detector. A concave grating with variable-line-spacing dispersed the HHG beam towards a micro-channel plate (MCP)/phosphor screen assembly, where the extreme ultraviolet (XUV) spectrum was recorded with a CCD camera.

As we described in [27], this setup enabled the generation of a strong continuum up to 160 eV with a flux of 10^9 photons/s. For the current study we replaced the 6 mm generation cell by a 2 mm long gas cell. The 2 mm cell is short enough to better preserve fingerprints of the cycle-to-cycle high-harmonic generation process. In the experiment, the results of which we analyze in detail here, we generated harmonics in 245 Torr Ne using 1.58 mJ NIR and 0.46 mJ MIR pulses. Similarly to our previous experiments [27], the MIR beam waist diameter was adjusted using a telescope to reach similar focused spot sizes. This meant an approximated peak intensity of the MIR beam that is $\sim 1/3$ of the NIR beam. We varied the delay between the two, while integrating the generated harmonic spectrum for 100 shots at each delay.

B. Experimental results and theoretical modeling

The recorded spectra as a function of the delay between the two pulses are shown in Fig. 2. We observe in Fig. 2(a) that at large delays, with no overlap between the two pulses, NIR-alone harmonics are observable which consist of narrow lines – as expected when harmonics are produced by a many-cycle pulse. In this configuration the MIR pulse alone does not produce any harmonics that are observable in the spectrum, due to the smaller intensity and different phase-matching conditions for each pulse alone. In temporal overlap, cutoff extension, yield enhancement and continuum spectra is observed, reported previously also by others [20, 21, 27]. Additionally, there are spectral shifts of harmonics appearing when the two pulses start to temporally overlap. This temporal region is shown in Fig. 2(b), where a stronger redshifted and a weaker blueshifted branch of harmonics are apparent, indicated by the red dashed and blue dotted curves, respectively. In similar experiments performed by Calegari et al. [20], these red- and blueshifted harmonics were observed before, while in the results of Siegel et al. the blue shift is more visible [21]. This is an effect that — to the best of our knowledge — has not been discussed so far, and forms the basis for our discussion in the remainder of the paper (see below).
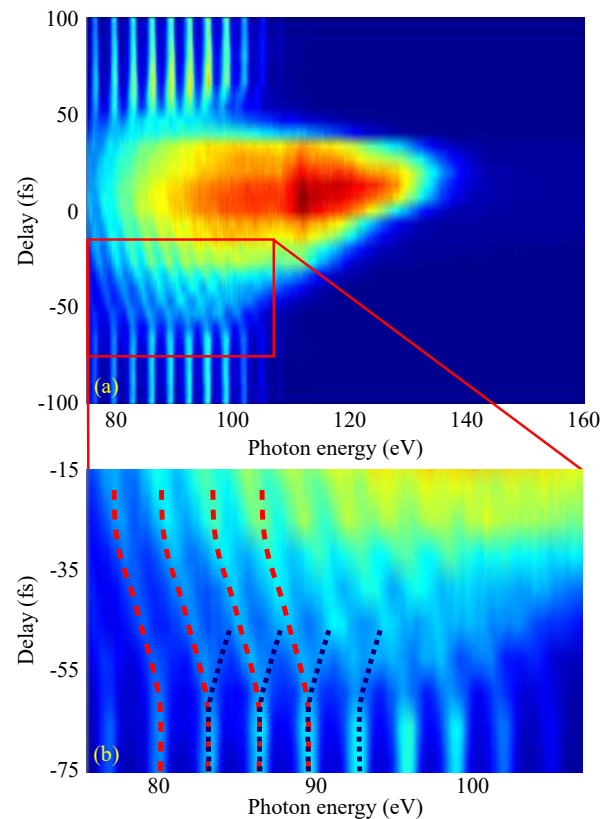

Fig. 2. (a) Experimental delay scan of the generated harmonic spectra. Negative delay means that the NIR pulse arrives before the MIR pulse. (b) Segment of the delay scan highlighted by the red box in (a), illustrating the observed redshifts (red dashed curves) and blueshifts (blue dotted curves) of the harmonic peaks.

To investigate the underlying physics behind the observed features, we used single-atom calculations (based on the Strong Field Approximation). The saddle-point approximation of the

Lewenstein integral [29, 30] was applied to calculate the relevant electron trajectories. Macroscopic conditions are taken into consideration by summing the results only for the relevant trajectories: (1) we consider only short trajectories, as these are usually better phase-matched in experiments, and (2) we limit emission to two half-cycles, before the peak of the pulse. The second assumption, the introduction of a temporal gate for emission, is explained in the following, while further reasons will be given for both assumptions later.

The combination of the two infrared fields severely limits the number of emission events at high photon energies by creating a field with a periodicity of 6.5 fs. Our previous macroscopic modeling of the propagation of the NIR and MIR laser pulses through the medium indicated that the generating pulses are severely distorted during propagation [27]. We have also observed that the ionization produced by the combined electric field has a very sharp rising time [28]. As phase-matching conditions depend strongly on the ionization rate, we expect a strong time dependence of phase-matching conditions, limiting efficient emission to only a few optical cycles of the generating pulse [31, 32]. This assumption has been verified in our previous work [27], where we concluded that efficient transient phase-matching may lead to the generation of isolated attosecond pulses in the present setup. In the experiment of Fig. 2 this is indicated by the measurement of a continuum spectrum in case of temporal overlap. This is the gating effect which we assumed in the calculations. The use of this rather crude model is justified by the nice illustration of the underlying physics that it provides. While the harmonic shifts of Fig. 2(b) were also visible in simulations carried out with a three-dimensional non-adiabatic simulation code (same as in [27, 28]), we describe here the simplified model, since it gives a more intuitive explanation for the results.

3. DISCUSSION

A. Two-color HHG with infinitely long driving fields and with limited radiation events

Both distortion of the laser pulses and transient phase-matching [27, 31, 32] affect the coherent build-up of emission at the rising edge of the pulse. Both effects are especially important when the generation involves pulses in the MIR spectral region, which are more sensitive to the presence of free electrons. To understand the process by which the MIR pulse influences the phase of the generated harmonics, we calculated the Lewenstein integral in the saddle-point approximation. Both fields were taken with cosine temporal evolution, i.e. $E_{NIR} = A_{NIR} \cos[\omega_{NIR} t]$ and $E_{MIR} = A_{MIR} \cos[\omega_{MIR}(t + \Delta t)]$, where A_{NIR} and A_{MIR} are field amplitudes, and Δt is a time delay (see Fig. 3(a)). In order to analyze and interpret the results, we only consider radiation corresponding to recombination events from short trajectories that are originated from a single optical cycle of the NIR field (1 NIR o.c.). This windows is highlighted with the white area in Fig. 3(a). With these assumptions, we analyze the effect of the weaker MIR field on the HHG process.

The results of the temporally gated single-atom calculations are illustrated in Fig. 3(b). We observe that the spectral lines shift with the 4.4 fs period of the MIR field (see Fig. 3(c)), and that the oscillation amplitude increases with harmonic order. There is also a variation of the harmonic yield with the same periodicity (see Fig. 3(d)). We note that the harmonic-yield maxima (minima) almost coincide with the maximum red(blue)shift of the harmonic peak positions. One could also notice that the ratio of the two field amplitudes (A_{NIR}/A_{MIR}) are approximately an
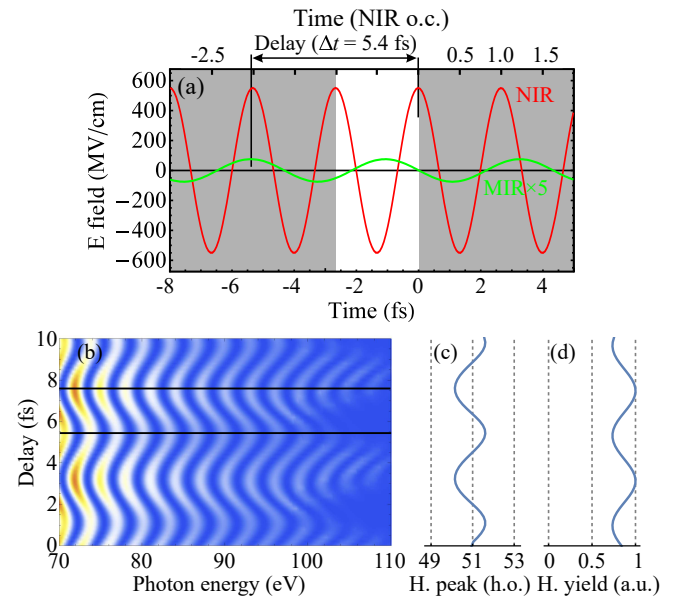

Fig. 3. (a) Temporal evolution of the monochromatic NIR (red) and MIR (green) electric fields used for calculation of the Lewenstein integral. (b) Single-atom harmonic spectra generated by the two fields at different MIR delays. In the calculations we only sum two short trajectory branches in a single optical cycle of the NIR field (highlighted by the white area in (a)). Two delays at the maximum blueshift (5.4 fs) and redshift (7.6 fs) are indicated with black horizontal lines. (c) Variation of the harmonic peak position with the delay. (d) Variation of the single-harmonic yield (51st harmonic, ∼ 79 eV) with the delay.

order of magnitude higher than the $A_{\text{NIR}}/A_{\text{MIR}} \approx 1.73$ value corresponding to the intensity ratio of ≈ 3 of the experiment. The reason for this deviation is given later.

The shift of the harmonic peaks with the delay can be understood by monitoring the electron trajectories producing the radiation. In Fig. 4 we plot the ionization and return times of the short trajectories in the temporal window corresponding to a single optical cycle of the NIR field (1 NIR o.c.) for the case where a maximum blueshift and minimum harmonic yield occur ($\Delta t = 5.4$ fs, Fig. 4(a) and (c)) and the case where a maximum redshift and a maximum harmonic yield occur ($\Delta t = 7.6$ fs, Fig. 4(b) and (d)). The main effect to consider is the relative strength of the total (NIR+MIR) field in the considered half-cycles, affecting both the relative delay and the strength of the generated harmonics. For a delay of $\Delta t = 5.4$ fs the NIR and MIR fields add destructively, and the trajectory analysis indicates that in particular in the second half-cycle the cutoff energy is higher. Extracting the emission times for the 51st harmonic (~ 79 eV) reveals that the time difference between the emission events in the consecutive two half-cycles is $\Delta T = 1.3$ fs $= 0.486$ NIR o.c.. This decreased time difference between the two events compared to the $\Delta T = 1.33$fs $= 0.5$ NIR o.c. of the MIR-free case means that constructive interference between the two XUV bursts occurs at a slightly higher XUV frequency, leading to a blueshift of the harmonic [15]. For a delay of $\Delta t = 7.6$ fs of the fields, we observe the opposite effect: there is a lower cutoff energy in the second half-cycle and a $\Delta T = 1.36$ fs $= 0.512$ NIR o.c. difference between the emission of the 51st harmonic in the two half-cycles. We note here that since the periodicities of the two fields are not multiples of each other, this effect is only observable if we limit the effective generation of the harmonics to a few half-cycles. The choice of a single cycle can be considered as a minimum value, since at least two emission events are necessary for these interference effects to be visible, and this is the reason for this specific selection of window size. At the same time, two optical cycles, e.g., would still allow the observation of these spectral shifts according to our single-atom calculations. Nevertheless, these effects will average out if multiple cycles were taken into account.

A similar spectral-shift effect is observable in HHG by a single short pulse [33–35]. Since the intensity varies considerably between half-cycles, the interference of the different emissions leads to a blueshift on the rising, and a redshift in the tailing part of the pulse. Since HHG emission is typically limited to the rising edge of the fundamental pulse (either via depletion [36, 37] or transient phase-matching [27, 31, 32]), a blueshift of harmonics is the observable effect of the described phenomenon with single-color generation. Moreover, distortions of the fundamental field and changes in its central frequency can cause spectral shifts of the generated harmonics [38]. In this work we describe additional spectral shifts, which have a bigger effect on the positions of the spectral peaks.

In addition to the photon-energy shift of harmonics illustrated in Fig. 3(c), there is also a periodic modulation of the harmonic yield (see Fig. 3(d)). This effect can be well understood if we consider the total field strength (NIR+MIR) at the times the ionization events happen. For the 5.4 fs delay case, the NIR and MIR fields have opposite sign in the time interval when the ionization of the electrons with the highlighted trajectories happens (see Fig. 4(a) and (c)). So, we can expect a reduced ionization probability, and a reduced harmonic yield, compared to the NIR-only case. This means the rate decreases when the harmonics suffer a blueshift. In contrast, in the 7.6 fs
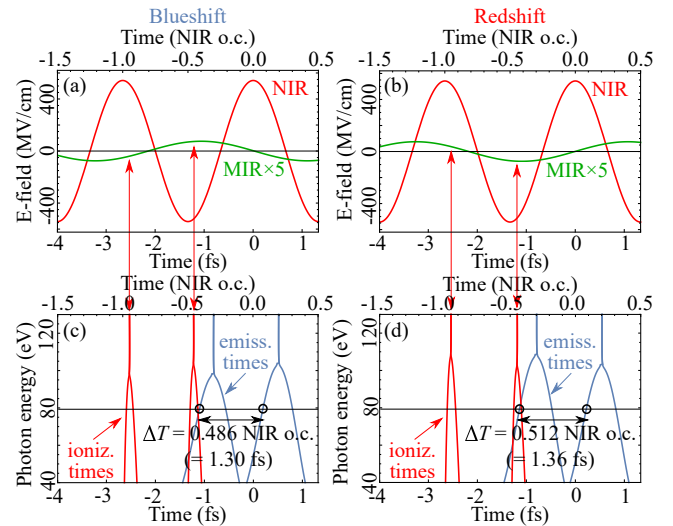

Fig. 4. (a-b) NIR and MIR electric fields at the two delays indicated in Fig. 3(b) corresponding to maximum blueshift (5.4 fs delay) and maximum redshift (7.6 fs delay) of the harmonic peaks. (c-d) Ionization and emission times of the considered trajectories. The photon energy corresponding to the 51st harmonic considered in Fig. 3(c) is indicated as a horizontal line.

delay case the ionization events correspond to instants when the two fields add constructively (see Fig. 4(b) and (d)). Therefore the emission rate increases while the harmonic peak is shifted downward (redshift).

B. Two-color HHG driven by short pulses

Now we discuss a similar scenario to the one described in the previous section, but instead of waves with a constant amplitude we consider temporally limited, many-cycle NIR and MIR pulses with a variable time delay between them. This allows for more direct comparison with the experimental situation described in Section 2. We still impose the time gate for ionization events indicated by the white area in Fig. 5(a), which temporally restricts the high-harmonic emission. The specific choice of the window position (-5 NIR o.c.) is based on the experimentally observed delay at which the harmonic shifts start to appear. When a later time window of the emission is chosen, the temporal delay at which the MIR field is strong enough to modify the trajectories shifts to earlier times (larger negative delays), since negative delay means that the NIR pulse arrives before the MIR pulse. An earlier window position leads to the opposite result, namely. the appearance of harmonic shifts at smaller negative delays. The chosen -5 NIR o.c. as emission window position fits best the experimental observations. The considered radiation is limited to contributions originating from short trajectories, like previously. Our simulations showed that while this selection is not crucial (e.g., long trajectories alone also give similar results), the spectral shifts are more clearly visible with short trajectory components alone. In the presence of all trajectories, they are almost totally blurred. This can be explained by the different influence of the assisting field on trajectories, leading to different interferences in the spectral domain. Since in our experiments we clearly see the spectral shifts, we restrict our analysis to short trajectories.

As it can be seen in Fig. 5(a), when the delay between the two pulses is decreasing, that is, they start to temporally overlap,
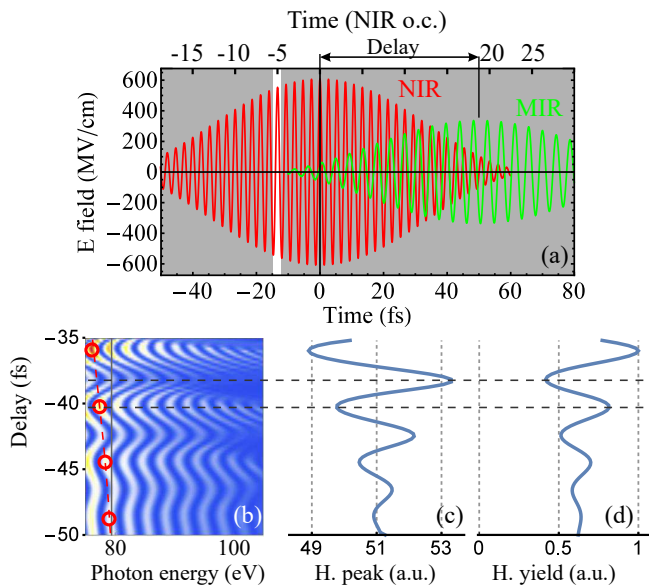
an increasing amplitude of the assisting MIR pulse falls into the temporal window. Thus the magnitude of the shifts of the harmonic peaks increases (see Fig. 5(b) and (c)). As the red-shifted harmonic yield is higher due to constructive interference between the two pulses as explained above (see Fig. 5(d)), their contribution into the final spectrum are stronger, and a stronger redshifted branch of the harmonic peaks can be observed when decreasing the delay (see the connected red circles in Fig. 5(b)).

It is also visible in Fig. 5(a) that at delays for which the spectral shifts are apparent in a broad frequency range (e.g., between $-50\,\text{fs}$ and $-35\,\text{fs}$, see Fig. 2(b)), the ratio of NIR and MIR field strengths is much larger (by approximately an order of magnitude) in the relevant emission window (the temporal domain marked by the white background in Fig. 5(a)) than the peak electric field ratio of the two pulses. This is the reason for the bigger $A_{\text{NIR}}/A_{\text{MIR}}$ amplitude ratio used in the simulation with monochromatic fields in the previous section.
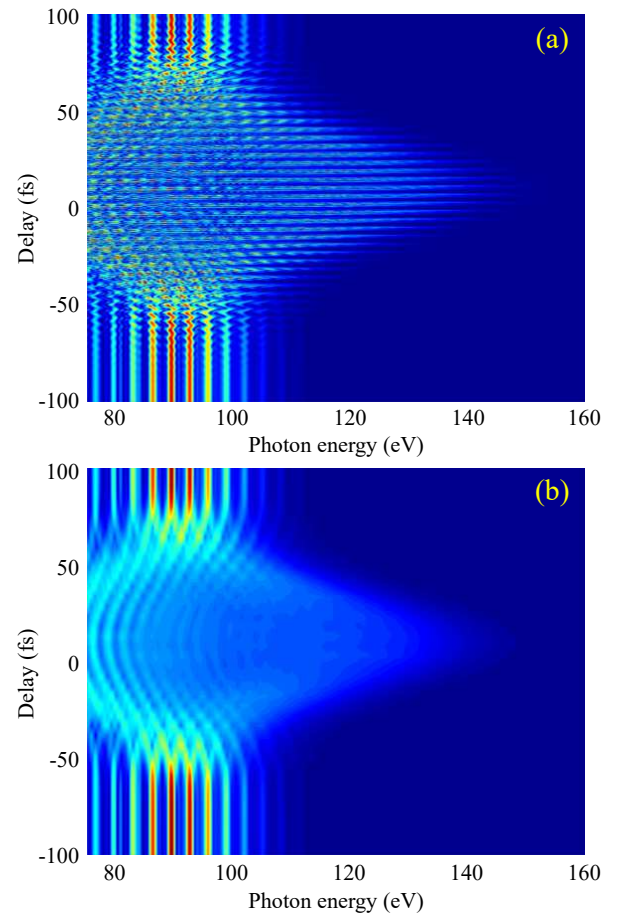

Fig. 5. (a) Temporal evolution of the generating NIR (red) and MIR (green) pulses for a negative NIR-MIR delay. We indicate with the white area a temporal gate that is taken into account – like in our previous calculations – for the high harmonic generation, in order to explain the physical mechanisms at play. (b) Single-atom harmonic spectra generated by the two fields of (a) at different MIR delays. The red circles indicate the delay values at which the oscillation of the yield and redshift of 51st ($\sim 79\,\text{eV}$) harmonic with delay reach a peak. (c) Oscillation of the harmonic peak position of the 51st harmonic emitted within the imposed temporal emission gate, and (d) the oscillation of the yield, both as a function of the NIR-MIR delay.

Fig. 6. (a) Single-atom response obtained by calculating the Lewenstein integral at different delays of the generating pulses with a temporal gate at $-5\,\text{NIR}$ o.c., each step for fixed values of the CEP of the NIR and MIR pulses (CEP = 0). (b) Single atom response as a function of delay with the same temporal gate, but with the spectra at each delay averaged over 13 shots with a random CEP between the NIR and MIR pulses.

In the experimentally recorded delay-scan (Fig. 2) the red- and blueshifts of the harmonics seem to be continuously changing with delay, leading to the two separate branches of shifted harmonic peaks highlighted in Fig. 2(b). Since this is not visible

in the results of Fig. 5(b), in order to explain these apparent shifts with delay, we performed further simulations with conditions replicating additional features of the experiments.

The calculations presented in Fig. 6 are based on calculating the Lewenstein integral (single-atom response) for different delays between the generating pulses and with a temporal gate (see Fig. 6(a)). To obtain these results, we applied a window function (a Tukey window instead of the previous top-hat, better reflecting real situations) to the generated dipole before calculating the spectrum. The window is centered at -5 NIR o.c. from the peak of the NIR field (at the rising edge), and it has a flat 1 NIR o.c. wide top, sinusoidally decreasing at the wings. In Fig. 6(a), like for the simulations before, it wa assumed that the two pulses have a fixed carrier-envelope phase (CEP $= 0$), and the delay between them is stable. The obtained results show similar characteristics to that of Fig. 5(b), showing that at delays producing maximum redshift of a harmonic approsimately overlap with the delays of maximum yield (see red circles in Fig. 5(b)).

For a better reproduction of the experimental results in Fig. 2, calculations were repeated assuming that the delay between the two pulses is not perfectly stable but is fluctuating between 0 and 7 fs with an RMS of 1.5 fs, the latter corresponding to the temporal step used experimentally. Based on this, we calculate an average spectrum for each delay by averaging spectra calculated over 13 more closely spaced delays, reproducing the experimental scans (see Fig. 6(b)). We observe in Fig. 6(b) the pronounced redshift in the temporally gated single-atom calculations, along with a separate branch of the less prominent blueshifted harmonics, similarly to the experimentally obtained spectra of Fig. 2. The results presented in Fig. 6(b) show that the apparent separation of harmonics to blue- and redshifted branches with decreasing delay between the two pulses is a result of an averaging effect. This is because the maximally blue- and redshifted harmonics are stronger (see Fig. 6(a) around -50 fs delay, which is the delay where separation is seen to begin in Fig. 6(b)).

One might also assume that the apparent continuous shift of harmonic peaks with delay is because of the low delay-step resolution of the experiment. However, the limited resolution of delay would only result in a continuous spectral shift, if the step size of delay (6.7 fs in the experiment) coincided with the periodicity of the MIR field (4.4 fs for the 1300 nm pulse) according to the single-atom calculations. If the two were equal, the oscillating shift with increasing amplitude (see Fig. 5(b)) would be sampled in a way that would appear as a continuously increasing amount of harmonic shift (like a sampling at delays shown with red circles in Fig. 5(b)). When the sampling and oscillation period are not the same, like in our experiment, single-atom results obtained using CEP-stable pulses do not show a continuous spectral shift of harmonics, but randomly varying spectral features with delay. So in our experiments, the combination of a fluctuating CEP and multi-shot acquisition contributed to the observed spectral features. We also note that our macroscopic simulations assuming a stable CEP suggest that volumetric averaging effects (serving as a kind of phase averaging) can result in similar, although less clear, appearance of continuous shifts with delay. This can lead to similar observations with CEP-stable pulses, like in a previous work [20].

4. CONCLUSIONS

We studied high-order harmonic generation by the combination of an 800 nm and a weaker 1300 nm driving pulse. We found

that the delay between the two pulses has a strong influence on the generated spectra. As the observed harmonic radiation is the interference of the elementary events from each half-cycle, the spectral structures are determined by the relative phases of these elementary emissions. The experimentally observed shift of the harmonic peaks with the delay can be well described by the effect of the weak MIR field on the phase of the generated harmonics.

REFERENCES

1. Z. Chang and P. Corkum, "Attosecond photon sources: the first decade and beyond [Invited]," Journal of the Optical Society of America B: Optical Physics **27**, B9–B17 (2010).
2. F. Calegari, G. Sansone, S. Stagira, C. Vozzi, and M. Nisoli, "Advances in attosecond science," Journal of Physics B: Atomic, Molecular and Optical Physics **49**, 062001 (2016).
3. S. Kühn, M. Dumergue, S. Kahaly, S. Mondal, M. Füle, T. Csizmadia, B. Farkas, B. Major, Z. Várallyay, F. Calegari, M. Devetta, F. Frassetto, E. Mansson, L. Poletto, S. Stagira, C. Vozzi, M. Nisoli, P. Rudawski, S. Maclot, F. Campi, H. Wikmark, C. L. Arnold, C. M. Heyl, P. Johnsson, A. L'Huillier, R. Lopez-Martens, S. Haessler, M. Bocoum, F. Boehle, A. Vernier, G. Iaquaniello, E. Skantzakis, N. Papadakis, C. Kalpouzos, P. Tzallas, F. Lépine, D. Charalambidis, K. Varjú, K. Osvay, and G. Sansone, "The ELI-ALPS facility: the next generation of attosecond sources," Journal of Physics B: Atomic, Molecular and Optical Physics **50**, 132002 (2017).
4. M. Chini, K. Zhao, and Z. Chang, "The generation, characterization and applications of broadband isolated attosecond pulses," Nature Photonics **8**, 178–186 (2014).
5. F. Krausz and M. I. Stockman, "Attosecond metrology: from electron capture to future signal processing," Nature Photonics **8**, 205–213 (2014).
6. F. Lepine, M. Y. Ivanov, and M. J. J. Vrakking, "Attosecond molecular dynamics: fact or fiction?" Nature Photonics **8**, 195–204 (2014).
7. K. Ramasesha, S. R. Leone, and D. M. Neumark, "Real-time probing of electron dynamics using attosecond time-resolved spectroscopy," Annual Review of Physical Chemistry **67**, 41–63 (2016).
8. M. Schultze, M. Fieß, N. Karpowicz, J. Gagnon, M. Korbman, M. Hofstetter, S. Neppl, A. L. Cavalieri, Y. Komninos, T. Mercouris, C. A. Nicolaides, R. Pazourek, S. Nagele, J. Feist, J. Burgdörfer, A. M. Azzeer, R. Ernstorfer, R. Kienberger, U. Kleineberg, E. Goulielmakis, F. Krausz, and V. S. Yakovlev, "Delay in photoemission," Science **328**, 1658–1662 (2010).
9. R. Pazourek, S. Nagele, and J. Burgdörfer, "Attosecond chronoscopy of photoemission," Reviews of Modern Physics **87**, 765–802 (2015).

10. P. M. Kraus, B. Mignolet, D. Baykusheva, A. Rupenyan, L. Horný, E. F. Penka, G. Grassi, O. I. Tolstikhin, J. Schneider, F. Jensen, L. B. Madsen, A. D. Bandrauk, F. Remacle, and H. J. Wörner, "Measurement and laser control of attosecond charge migration in ionized iodoacetylene," Science **350**, 790–795 (2015).

11. F. Calegari, A. Trabattoni, A. Palacios, D. Ayuso, M. C. Castrovilli, J. B. Greenwood, P. Decleva, F. Martín, and M. Nisoli, "Charge migration induced by attosecond pulses in bio-relevant molecules," Journal of Physics B: Atomic, Molecular and Optical Physics **49**, 142001 (2016).

12. J.-C. Diels and W. Rudolph, *Ultrashort Laser Pulse Phenomena* (Academic Press, 2006), 2nd ed.

13. K. T. Kim, C. Zhang, T. Ruchon, J.-F. Hergott, T. Auguste, V. M., C. B., and QuereF., "Photonic streaking of attosecond pulse trains," Nature Photonics **7**, 651–656 (2013).

14. J. Mauritsson, P. Johnsson, R. López-Martens, K. Varjú, W. Kornelis, J. Biegert, U. Keller, M. B. Gaarde, K. J. Schafer, and A. L'Huillier, "Measurement and control of the frequency chirp rate of high-order harmonic pulses," Physical Review A: Atomic, Molecular, and Optical Physics **70**, 021801 (2004).

15. K. Varjú, Y. Mairesse, B. Carré, M. B. Gaarde, P. Johnsson, S. Kazamias, R. López-Martens, J. Mauritsson, K. J. Schafer, P. Balcou, A. L'huillier, and P. Salières, "Frequency chirp of harmonic and attosecond pulses," Journal of Modern Optics **52**, 379–394 (2005).

16. S. Watanabe, K. Kondo, Y. Nabekawa, A. Sagisaka, and Y. Kobayashi, "Two-color phase control in tunneling ionization and harmonic generation by a strong laser field and its third harmonic," Physical Review Letters **73**, 2692–2695 (1994).

17. I. Kim, H. Kim, C. Kim, J. Park, Y. Lee, K.-H. Hong, and C. Nam, "Efficient high-order harmonic generation in a two-color laser field," Applied Physics B **78**, 859–861 (2004).

18. D. B. Milošević, W. Becker, and R. Kopold, "Generation of circularly polarized high-order harmonics by two-color coplanar field mixing," Physical Review A: Atomic, Molecular, and Optical Physics **61**, 063403 (2000).

19. O. Kfir, P. Grychtol, E. Turgut, R. Knut, D. Zusin, D. Popmintchev, T. Popmintchev, H. Nembach, J. M. Shaw, A. Fleischer, H. Kapteyn, M. Murnane, and O. Cohen, "Generation of bright phase-matched circularly-polarized extreme ultraviolet high harmonics," Nature Photonics **9**, 99–105 (2015).

20. F. Calegari, C. Vozzi, M. Negro, G. Sansone, F. Frassetto, L. Poletto, P. Villoresi, M. Nisoli, S. D. Silvestri, and S. Stagira, "Efficient continuum generation exceeding 200 ev by intense ultrashort two-color driver," Optics Letters **34**, 3125–3127 (2009).

21. T. Siegel, R. Torres, D. J. Hoffmann, L. Brugnera, I. Procino, A. Zaïr, J. G. Underwood, E. Springate, I. C. E. Turcu, L. E. Chipperfield, and J. P. Marangos, "High harmonic emission from a superposition of multiple unrelated frequency fields," Optics Express **18**, 6853–6862 (2010).

22. E. J. Takahashi, P. Lan, O. D. Mücke, Y. Nabekawa, and K. Midorikawa, "Infrared two-color multicycle laser field synthesis for generating an intense attosecond pulse," Physical Review Letters **104**, 233901 (2010).

23. C. Jin, G. Wang, A.-T. Le, and C. D. Lin, "Route to optimal generation of soft x-ray high harmonics with synthesized two-color laser pulses," Scientific Reports **4**, 7067 (2014).

24. J. Mauritsson, P. Johnsson, E. Gustafsson, A. L'Huillier, K. J. Schafer, and M. B. Gaarde, "Attosecond pulse trains generated using two color laser fields," Physical Review Letters **97**, 013001 (2006).

25. X. He, J. M. Dahlström, R. Rakowski, C. M. Heyl, A. Persson, J. Mauritsson, and A. L'Huillier, "Interference effects in two-color high-order harmonic generation," Physical Review A: Atomic, Molecular, and Optical Physics **82**, 033410 (2010).

26. C. Chen, C. Hernández-García, Z. Tao, W. You, Y. Zhang, D. Zusin, C. Gentry, P. Tengdin, A. Becker, A. Jaron-Becker, H. Kapteyn, and M. Murnane, "Influence of microscopic and macroscopic effects on attosecond pulse generation using two-color laser fields," Optics Express **25**, 28684–28696 (2017).

27. B. Schütte, P. Weber, K. Kovács, E. Balogh, B. Major, V. Tosa, S. Han, M. J. J. Vrakking, K. Varjú, and A. Rouzée, "Bright attosecond soft X-ray pulse trains by transient phase-matching in two-color high-order harmonic generation," Optics Express **23**, 33947–33955 (2015).

28. K. Kovacs, V. Tosa, B. Major, E. Balogh, and K. Varju, "High-efficiency single attosecond pulse generation with a long-wavelength pulse assisted by a weak near-infrared pulse," IEEE Journal of Selected Topics in Quantum Electronics **21**, 1–7 (2015).

29. G. Sansone, C. Vozzi, S. Stagira, and M. Nisoli, "Nonadiabatic quantum path analysis of high-order harmonic generation: Role of the carrier-envelope phase on short and long paths," Physical Review A: Atomic, Molecular, and Optical Physics **70**, 013411 (2004).

30. E. Balogh, J. Fülóp, J. Hebling, P. Dombi, G. Farkas, and K. Varjú, "Application of high intensity thz pulses for gas high harmonic generation," Central European Journal of Physics **11**, 1135–1140 (2013).

31. M.-C. Chen, C. Mancuso, C. Hernández-García, F. Dollar, B. Galloway, D. Popmintchev, P.-C. Huang, B. Walker, L. Plaja, A. A. Jaroń-Becker, A. Becker, M. M. Murnane, H. C. Kapteyn, and T. Popmintchev, "Generation of bright isolated attosecond soft X-ray pulses driven by multicycle midinfrared lasers," Proceedings of the National Academy of Sciences **111**, E2361–E2367 (2014).

32. C. Hernández-García, T. Popmintchev, M. M. Murnane, H. C. Kapteyn, L. Plaja, A. Becker, and A. Jaron-Becker, "Isolated broadband attosecond pulse generation with near- and mid-infrared driver pulses via time-gated phase matching," Optics Express **25**, 11855–11866 (2017).

33. C. M. Heyl, J. Güdde, U. Höfer, and A. L'Huillier, "Spectrally resolved maker fringes in high-order harmonic generation," Physical Review Letters **107**, 033903 (2011).

34. L. He, P. Lan, Q. Zhang, C. Zhai, F. Wang, W. Shi, and P. Lu, "Spectrally resolved spatiotemporal features of quantum paths in high-order-harmonic generation," Physical Review A: Atomic, Molecular, and Optical Physics **92**, 043403 (2015).

35. P. Lan, M. Ruhmann, L. He, C. Zhai, F. Wang, X. Zhu, Q. Zhang, Y. Zhou, M. Li, M. Lein, and P. Lu, "Attosecond probing of nuclear dynamics with trajectory-resolved high-harmonic spectroscopy," Physical Review Letters **119**, 033201 (2017).

36. M. J. Abel, T. Pfeifer, P. M. Nagel, W. Boutu, M. J. Bell, C. P. Steiner, D. M. Neumark, and S. R. Leone, "Isolated attosecond pulses from ionization gating of high-harmonic emission," Chemical Physics **366**, 9–14 (2009).

37. F. Ferrari, F. Calegari, M. Lucchini, C. Vozzi, S. Stagira, G. Sansone, and M. Nisoli, "High-energy isolated attosecond pulses generated by above-saturation few-cycle fields," Nature Photonics **4**, 875–879 (2010).

38. Y. Tamaki, J. Itatani, Y. Nagata, M. Obara, and K. Midorikawa, "Highly efficient, phase-matched high-harmonic generation by a self-guided laser beam," Physical Review Letters **82**, 1422–1425 (1999).